Available online at www.sciencedirect.com
SCIENCE DIRECT®
Lithos 74 (2004) 1–20
LITHOS
www.elsevier.com/locate/lithos

The thermal regimes of the upper mantle beneath Precambrian and Phanerozoic structures up to the thermobarometry data of mantle xenoliths

V.A. Glebovitsky, L.P. Nikitina, V.Ya. Khiltova, N.O. Ovchinnikov*

Institute of Precambrian Geology and Geochronology, Russian Academy of Sciences, nab. Makarova 2, St. Petersburg, 199034, Russia

Received 29 January 2003; accepted 27 March 2003

Abstract

The thermal state of the upper mantle beneath tectonic structures of various ages and types (Archaean cratons, Early Proterozoic accretionary and collisional orogens, and Phanerozoic structures) is characterized by geotherms and by thermal gradients (TG) derived from data on the $P-T$ conditions of mineral equilibria in garnet and garnet–spinel peridotite xenoliths from kimberlites (East Siberia, Northeastern Europe, India, Central Africa, North America, and Canada) and alkali basalts (Southeastern Siberia, Mongolia, southeastern China, southeastern Australia, Central Africa, South America, and the Solomon and Hawaiian islands). The use of the same garnet–orthopyroxene thermobarometer (Theophrastus Contributions to Advanced Studies in Geology. 3: Capricious Earth: Models and Modelling of Geologic Processes and Objects 2000 44) for all xenoliths allowed us to avoid discrepancies in estimation of the $P-T$ conditions, which may be a result of the mismatch between different thermometers and barometers, and to compare the thermal regimes in the mantle in various regions. Thus, it was established that (1) mantle geotherms and geothermal gradients, obtained from the estimation of $P-T$ equilibrium conditions of deep xenoliths, correspond to the age of crust tectonic structures and respectively to the time of lithosphere stabilization; it can be suggested that the ancient structures of the upper mantle were preserved within continental roots; (2) thermal regimes under continental mantle between the Archaean cratons and Palaeoproterozoic belts are different today; (3) the continental mantle under Neoproterozoic and Phanerozoic belts is characterized by significantly higher values of geothermal gradient compared to the mantle under Early Precambrian structures; (4) lithosphere dynamics seems to change at the boundary between Early and Mezo-Neoproterozoic and Precambrian and Phanerozoic.

Keywords: Mantle; Xenoliths; Thermobarometry; Upper mantle; Geotherms; Thermal gradients; Thermal state

1. Introduction

The study of the thermal state of the continental mantle and the spatial–temporal heterogeneity of its thermal regimes is relevant in the context of the lithospheric evolution problem and the elucidation of when and where the first stable regions of continental mantle appeared, how long they persisted, and how the processes forming the mantle and the crust are interrelated (Pearson, 1999). To solve these problems, it is important to clarify whether the thermal regimes in the mantle beneath

* Corresponding author. Tel.: +7-812-3280362; fax: +7-812-3284801.
E-mail address: Nikita@no8266.spb.edu (N.O. Ovchinnikov).

0024-4937/$ - see front matter © 2004 Elsevier B.V. All rights reserved.
doi:10.1016/j.lithos.2003.03.001

Precambrian and Phanerozoic structures are different and whether the thermal state of the mantle correlates with the type and age of tectonic structures in the crust. The existence of a correlation between geothermal regimes in the mantle and the age of the last major thermal event in the crust (the tectonothermal age) is shown by Poudjom Djomani et al. (2001). They have constructed, or collected from the literature, xenolith/xenocryst-based palaeogeotherms for more them 300 localities worldwide, and classified these by their tectonothermal age. These empirically determined palaeogeotherms are typically low beneath Archaean cratonic areas (≥ 2.5 Ga), higher beneath Proterozoic regions ($2.5-1.0$ Ga), and still higher beneath areas of Phanerozoic tectonic activity.

It appears reasonable to use the same thermobarometric tool for estimating thermal regimes in the mantle underlying different types of structures in various continents such as Archaean cratons, Proterozoic collisional and accretionary belts, Phanerozoic accretionary belts, and rifts developing in the range of Precambrian and Phanerozoic structures. An opportunity to obtain such estimations is provided by xenoliths of mantle rocks in kimberlites, lamproites, and related rocks developed in Precambrian structures and by xenoliths in alkali basalts localized in Phanerozoic accretionary belts and in rifts.

In this paper, the thermal state of the mantle is characterized by geotherms in significant depth intervals and by thermal gradient (TG) values (TG = T/h, C/km, where h is depth in km; $h = 3.4P$, P is pressure in kbar), obtained from data on the $P-T$ conditions of mineral equilibria in xenoliths of garnet and garnet–spinel peridotites and garnet pyroxenites because the mineral composition of these rocks, including orthopyroxene and garnet, provides constraints on both the temperatures and pressures of crystallization. We use the same garnet–orthorpyroxene thermobarometer (Nikitina, 2000) for all xenoliths to avoid discrepancies in estimation of the $P-T$ conditions, which would otherwise result from the inconsistency of different thermometers and barometers, and to enable adequate comparison of thermal states of the continental mantle in widely spaced regions.

2. Garnet–orthopyroxene thermobarometer

The thermobarometer were calibrated using experimental data on the garnet–orthopyroxene equilibrium in the FMAS and CFMAS systems at 800, 900, 975, 1050, 1150, and 1200 °C and at pressures ranging from 5 to 30 kbar (Harley, 1984a,b) and taking into account thermodynamic data for the enstatite–ferrosilite series in a quasichemical model for multisublattice low-symmetry solid solutions (Nikitina, 1986; Nikitina and Ivanov, 1992). The interchange energy $\omega^{Opx}_{Fe\text{-}Mg} = -3300 \pm 500$ kal/mol. The simple ideal solution model was used for Mg–Al and Fe–Al mixtures in orthopyroxenes ($\omega^{Opx}_{Mg-Al} = \omega^{Opx}_{Fe-Al} = 0$). Pyrope–almandine solid solutions are considered to be ideal ($\omega^{Gr}_{Fe-Mg} = 0$) as well.

A thermometer based on the exchange reaction

$$MgSiO_3 + FeAl_{2/3}SiO_4 = FeSiO_3 + MgAl_{2/3}SiO_4$$

$$\begin{aligned} T = \{&[\ln K_{Fe} + 2.0909 - 3.2707x^{Opx}_{Fe} + 1.39(x^{Opx}_{Fe})^2 \\ &+ 0.2x^{Opx}_{Al} - 3.0(x^{Opx}_{Al})^2 - 0.9774x^{Gr}_{Ca}] \\ &/[-0.00078x^{Opx}_{Fe} - 0.00035x^{Gr}_{Ca} + 0.0007(x^{Gr}_{Ca})^2 \\ &+ 0.0022(x^{Gr}_{Ca})^3 + 0.000807]\} - 273 \end{aligned}$$

A barometer based on the reaction

$$(Mg_{1-n}Fe_n)_{1-p}Al_{2p}Si_{1-p}O_3 + Al_2O_3 \Rightarrow Mg_{1m}Fe_mAl_{2/3}SiO_4$$

$$\begin{aligned} P = {} & 0.04T + [7.8 - 41.3x^{Opx}_{Fe} + 10.1(x^{Opx}_{Fe})^2] \\ &+ [-399.5 + 36.5x^{Opx}_{Fe} + 385.1(x^{Opx}_{Fe})^2]x^{Opx}_{Al} \\ &+ [1408.7 + 518.9x^{Opx}_{Fe} - 2161.2(x^{Opx}_{Fe})^2](x^{Opx}_{Al})^2 \\ &+ [-6600 + 2500x^{Opx}_{Fe} + 11800(x^{Opx}_{Fe})^2](x^{Opx}_{Al})^3 \\ &+ 12000(x^{Opx}_{Al})^4 + [-8.5x^{Gr}_{Fe} - 6.5x^{Gr}_{Ca} \\ &+ 15.5(x^{Gr}_{Ca})^2] \end{aligned}$$

where T in °C and P in kbar;

$$K_{Fe} = x_{Fe}^{Opx}/x_{Fe}^{Gr};$$

$$x_{Fe}^{Opx} = Fe^{2+}\text{f.u.},$$

$$x_{Al}^{Opx} = 1/2(Al_{tot}^{Opx})\ \text{f.u. per formula } MSiO_3;$$

$$x_{Fe}^{Gr} = 1/3(Fe^{2+})\ \text{f.u.},$$

$$x_{Ca}^{Gr} = 1/3(Ca)\ \text{f.u. per formula } M_3Al_2Si_3O_{12}$$

The uncertainties in temperature and pressure are ± 10% and ± 5%, respectively.

Data of Table 1 show that this thermobarometer reproduces experimental conditions for natural garnet peridotites within the stated errors of temperature and pressure values. No systematic deviations of calculated P, T values from experimental data in the MAS system in the range of 10–40 kbar at 1000–1600 °C (MacGregor, 1974; Perkins et al., 1980) were observed. The validity of this thermobarometer version is supported also by comparison P–T conditions of peridotitic inclusions in diamonds and diamond- and graphite-bearing garnet peridotite formation with the diamond–graphite univariant curve (Bundy et al., 1961). The position on the P–T diagram of diamond-bearing (about 90%) and graphite-bearing rocks (Fig. 1) is in accordance with the stability fields of corresponding carbon modifications.

Table 1
Comparison of experimental and calculated by Gr–Opx thermobarometer temperature (°C) and pressure (kbar) values for garnet peridotites

Sample	Experimental		Calculated	
	T	P	T	P
N-8[a]	1100	31.0	985	37.9
N-13[a]	1100	38.0	1075	40.7
1315[b]	1150	30.0	1145	37.5
BK[c]	1400	60.0	1405	58.7
455[d]	1450	50.0	1465	49.4
494[d]	1400	50.0	1425	50.8
S-18[e]	1200	45.0	1240	45.9
N-6[c]	1200	45.0	1165	43.7

[a] Akella, 1976.
[b] Green and Adam, 1991.
[c] Brey and Kohler, 1990.
[d] Ryabchikov et al., 1993.
[e] Akaogi and Akimoto, 1979.

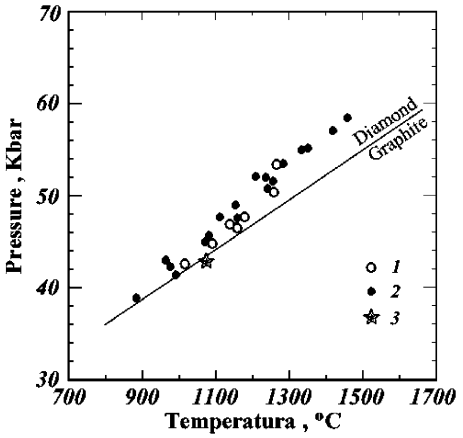

Fig. 1. P–T plot for peridotite inclusions in diamonds (1), diamond-bearing (2) and graphite-bearing (3) peridotite xenoliths. Mineral analyses are taken from Sobolev et al. (1976, 1984, 1997), Danchin and Boyd (1976), Gurney et al. (1979), Tsai et al. (1979), Laz'ko and Sharkov (1988), Rickard et al. (1989); and Carswell and Gibb (1998) (P, T values in Table 3). The curve of the polymorphic graphite–diamond transition is from Bundy et al. (1961).

This thermobarometer is suitable for determination the $P-T$ equilibrium conditions of the garnet–orthopyroxene assemblage from both basic and ultrabasic rocks virtually throughout the stability field of it [$700 \le T \le 1500$ °C and $(4–5) \le P \le (55–60)$ kbar]. The main advantage of this thermobarometer is that both parameters (T and P) are determined solely based on the garnet–orthopyroxene assemblage.

3. Study objects

In this paper, the investigation results of P–T equilibrium condition of garnet–orthopyroxene assemblages from peridotite and pyroxenite xenoliths in kimberlites and related rocks in East Siberia, Northeastern Europe (Archangelsk region and Finland), South Africa, India, and North America and alkali basalts in Central Africa, East Siberia, Mongolia, southeastern China, southeastern Australia, South America, and Hawaii and Malaita Islands (Fig. 2) are presented. They establish the thermal state of the lithospheric mantle underlying Precambrian and Phanerozoic tectonic structures of different types on

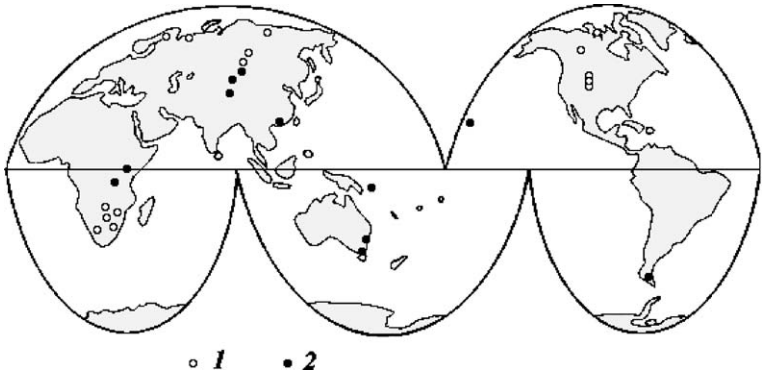

Fig. 2. Location of (1) kimberlite pipes and (2) alkali-basalt volcanoes from which the garnet peridotite xenoliths under study were sampled.

various continents, as well as on the thermal state of the oceanic lithospheric mantle. The type and age tectonic structures, where kimberlites and basalts are situated, are shown in Table 2.

The analytical data on the compositions of coexisting garnets and orthopyroxenes in xenoliths are taken from the literature.

4. Results

The estimation of the equilibrium temperatures and pressures (and, accordingly, depths) for xenoliths from kimberlites and alkali basalts and their corresponding TG values in the mantle are presented in Tables 3 and 4 and in Figs. 3 and 4. Geotherms of the upper mantle underlying various Precambrian and Phanerozoic structures are shown in Fig. 5.

Mantle xenoliths form two groups of geotherms in the $P-T$ diagram; one can be described as "cold," and the other as "hot."

The cold group includes geotherms derived from peridotite xenoliths in kimberlites and related rocks (alkali picrites, lamproites, minettes, and lamprohyres) and characterizes the thermal state of the mantle underlying Archaean cratons (cratons in the basement of the East Siberian platform, the Kuloisky and the Karelian cratons in Northeastern Europe, the Kaapvaal and the Zimbabwe cratons in South Africa, the Dharvar craton in India, the Wyoming, the Central Slave craton in North America and the Archaean craton in the basement of the Arctic platform on Somerset Island), Archaean (the Limpopo belt) and Proterozoic (the West Olenek belt in East Siberia, the Natal and Namaqualand belts in South Africa) collisional and accretionary belts (the Yavapi foldbelt in North America).

The geotherms of the "cold" group are described by linear equations, and they all cross the model continental geotherms consistent with heat flows of 40–45 mW/m^2 (Pollack and Chapman, 1977).

Considering the similarity of TG mantle values in full beneath each of the structures, we calculated their averages, which are presented in Table 2. The averages in the upper mantle are 7.2 ± 0.2 °C/km beneath the Archaean cratons of the East Siberian platform (the number of determinations $n = 54$); 7.4 ± 0.03 beneath Kuloisky craton ($n = 3$); 7.2 ± 0.1 beneath Karelian craton ($n = 13$); 7.2 ± 0.2 °C/km beneath the Kaapvaal craton ($n = 46$); and 7.3 ± 0.1 °C/km beneath the Dharvar craton ($n = 11$). However, we obtained significantly higher TG values (7.9 ± 0.3 °C/km; $n = 4$) for the mantle in the southernmost zone of the Wyoming craton, near its contact with the Proterozoic Yavapi accretionary belt. As can be seen from Table 2, they are typical of the upper mantle beneath Proterozoic tectonic structures rather than Archaean cratons. The mantle underlying the Central Slave craton and Archaean basement of the Arctic platform in Canada has similar values: the averages are 7.5 ± 0.1 °C/km, which may be due to the Proterozoic reworking of the Archaean cratons in these regions.

The TG averages in the mantle underlying Precambrian collisional belts are slightly higher than those for the mantle beneath Archaean cratons, but these differ-

ences are statistically significant. For the Early Proterozoic West Olenek belt in the northern part of the East Siberian platform the TG average is 7.5 ± 0.3 °C/km (n = 14). In South Africa, for Archaean Limpopo belt, the TG average is 7.6 ± 0.3 °C/km (n = 5), for the Middle Proterozoic belts the TG averages are equal to 7.4 ± 0.3 °C/km (Natal belt) and from 7.4 to 7.7 °C/km (Namaqualand: for the Louwrensia, Anis-Kubub, and Hanaus areas they are 7.4 ± 0.2, 7.6 ± 0.1, and 7.7 ± 0.3 °C/km, respectively).

The thermal regime in the mantle underlying the Early Proterozoic Yavapi accretionary belt in North America is characterized by higher TG values than in the mantle underlying the aforementioned collisional belts: the average TG there is 7.9 ± 0.4 °C/km (n = 14).

The "cold" group includes also geotherm derived from garnet peridotite xenoliths in Genozoic alkali basalts of the Labait and Lashaine volcanoes in Tanzania. The Labait volcano is situated in the Archaean Tanzanian craton near its boundary with the polycyclic collisional Mozambique belt (0.9–0.6 Ga), which consist of a region of reworked Archaean crust directly east of the craton (based on Sm–Nd model ages; Moller et al., 1998). Re–Os depletion ages for the mantle xenoliths from Labait yield minimum melt extraction ages up to ≈ 2.8 Ga, indicating that stabilization of the lithospheric mantle occurred by the end of the Archaean (Lee and Rudnick, 1999). The Lashaine volcano is situated in the Mozambique collisional belt near to the east boundary of Tanzanian craton. Both volcanoes are located in the Tanzanian section of the East African Rift. Pressure of 47.7–53.9 kbar and temperature of 1240–1450 °C characterize the crystallization conditions of peridotite xenoliths from basalts of Labait volcano. The peridotites supplied by basalts of Lashaine volcano yield pressures of 47.1–56.0 kbar and temperatures of 1210–1420 °C. The TG averages are 7.7 ± 0.1 °C/km (n = 12) and7.5 ± 0.1 °C/km (n = 10), respectively. Such TG values are typical of the mantle beneath Proterozoic collisional belts or marginal parts of Archaean cratons.

The "hot" group comprises geotherms derived from xenoliths of peridotites and pyroxenites in alkali basalts of the Vitim Upland in the Trans-Baikal region, the Tariat depression and Dariganga plateau in Mongolia, and southeastern China, as well as from xenoliths of alkali basalts and mugearite and alnoite dikes of southern and southeastern Australia, Tasmania and southeastern South America. Most of geotherms of this group describe thermal regimes in the upper mantle underlying Late Proterozoic and Phanerozoic accretionary belts (see Table 1); the only exception is the South Mongolia geotherm, which reflects the thermal state of the mantle under Hercynian collisional belt. This group also includes the geotherm derived from xenoliths in Hawaiian alkali basalts and characterizing the thermal state of the oceanic hotspot mantle.

Mantle geotherms in the southeastern South America (Phanerozoic belt) and the Vitim Plateau (ripheides of Central Asian belt) cross at small angles the continental geotherms corresponding to a heat flow of 50–60 mW/m^2 (Pollack and Chapman, 1977). Geotherms in Central Mongolia (caledonides of the Central Asian belt) and southeastern Australia (Tasmanian Palaeozoic belt) coincide with the 55 mW/m^2 geotherm, whereas the geotherm in southeastern China (Late Yangchuan Genozoic foldbelts) is close to the 60 mW/m^2 geotherm. The Hawaii geotherm is consistent with the oceanic model geotherm (Clark and Ringwood, 1964).

The TG averages in the mantle under regions containing alkali basalts are 9.0 ± 0.2 °C/km (South America; n = 17), 9.4 ± 0.3 °C/km (Vitim Plateau; n = 16), 9.4 ± 0.2 °C/km (Dariganga Plateau, n = 4), 10.0 ± 0.2 °C/km (Tariat depression; n = 15), 10.8 ± 0.5 °C/km (southeastern Australia; n = 23), 12.0 ± 0.5 °C/km (southeastern China; n = 13), and 11.7 ± 0.2 °C/km (Hawaii; n = 5).

Maximum values of pressure obtained for xenoliths in various types of Precambrian and Phanerozoic structures provide a possibility to calculate the maximum depths (Table 2) at which mantle xenoliths of garnet and garnet–spinel peridotites and garnet pyroxenites were incorporated into kimberlites and alkali basalts (or the minimum melting depths of kimberlite and alkali-basalt magmas). As can be seen from Fig. 6, there are two trends in the correlation between maximum depths and the TG averages in the mantle; one trend is characteristic of Precambrian structures, and the other is characteristic of Phanerozoic structures. For Phanerozoic structures, a distinct inverse correlation is observed between the maximum xeno-

Table 2
Type and age of tectonic structure, TG averages in the Upper mantle and maxima depths of the garnet-bearing peridotite and pyroxenite xenolith emplacements into kimberlites and basalts

Region	Type and age structure	*n*	TG (°C/km)	Depth (km)
Archaean cratons				
Central parts of the East Siberian kimberlite province (Mir and Udachnaya pipes)	Cratons in the basement of the East Siberian platform, 2.6 Ga (Neymark et al., 1992; Kovach et al., 2000)	54	7.1 ± 0.2	230
Northeastern Europe, Archangelsk region, the pipes of Simnii bereg	The basement of East European platform, Kuloi craton, (Sablukov et al., 2000)	3	7.4 ± 0.3	150
Finland, Kuopio and Kaavi pipes	Baltic shield, Karelian craton, 3.1–2.6 Ga, near its boundary with Svecofennian foldbelt, 1.9–1.8 Ga (Peltonen et al., 1999)	3	7.2 ± 0.1	155
South African kimberlites (Premier, Kimberley, Finsh, Koffiefontein, Bullfontein, Frank Smith, and Klippfontein)	Kaapvaal craton, 3.0 Ga (Anhaeusser, 1971; Kondie, 1981; Cohen et al., 1974)	46	7.2 ± 0.2	230
South Africa, Botswana kimberlites (Letlhakane pipes)	Zimbabwe craton, 3.6–2.5 Ga, near its boundary with Proterozoic Magondi fold-belt, 2.2–2.05 Ga (Stiefenhofer et al., 1997)	5	7.3 ± 0.1	180
Central Africa, Tanzania, Labait alkali-basalt Volcano	Tanzanian craton, 2.8 Ga (Lee and Rudnick, 1999), near its boundary with Mozambique foldbelt, 0.9–0.6 Ga; the Tanzanian section of the East African Rift (Dawson et al., 1997; Moller et al., 1998; Lee and Rudnick, 1999)	12	7.7 ± 0.1	185
India, Karnataka (Varjrakurer kimberlite pipes)	West Dharvar craton, about 3.0 Ga (Rai et al., 1996)	11	7.3 ± 0.1	180
North America, Montana kimberlite pipes	Wyoming craton, 3.1 Ga, near its boundary with the Lower Proterozoic Yavapi belt (Hoffman, 1989)	4	7.9 ± 0.3	170
Canada, Jericho kimberlite pipes	North Central Slave craton, 2.6 Ga (Fyson and Helmstaedt, 1988; Yamashita et al., 2000)	5	7.5 ± 0.1	150
Canada, Somerset Island kimberlites (Elwin Bay and Nikos pipes)	Arctic platform, the fragmented and re worked in Pt_1 craton, (Hoffman, 1989; Schmidberger and Francis, 1999)	14	7.5 ± 0.2	180
Precambrian foldbelts				
Collisional belts				
South Africa, Limpopo, Venetia kimberlite pipes	Limpopo foldbelt, Central zone, Archaean (Cox et al., 1989; Stiefenhofer et al., 1999)	5	7.6 ± 0.3	180
Northern part of the East Siberian platform, the Olenek uplift kimberlite province (the Obnazhennaya pipe)	West Olenek belt (Khiltova and Nikitina, 1997), 1.7 Ga (McCulloch, 1989)	14	7.5 ± 0.3	170
South Africa, Lesotho kimberlites (Northern Lesotho, Thaba Putsoa, and Kao pipes)	Contact zone of the Natal foldbelt with the Kaapvaal craton, 1.3–1.1 Ga (Peters, 1991)	19	7.4 ± 0.2	190
South Africa, Namilian kimberlites:	Contact zone of the Namaqualand foldbelt			
(1) Louwrensia pipes	with the Kaapvaal craton, 1.3–1.1 Ga	13	7.4 ± 0.1	195
(2) Annis-Kubub pipes	(Peters, 1991)	13	7.6 ± 0.1	175
(3) Hanaus pipes		33	7.7 ± 0.3	210
Central Africa, Tanzania, Lashaine alkali-basalt Volcano	Mozambique foldbelt, 0.9–0.6 Ga (Moller et al., 1998), near to the east boundary of Tanzanian craton; the Tanzanian section of the East African Rift (Dawson et al., 1997)	10	7.5 ± 0.1	190
Accretionary belts				
South America, Colorado kimberlites (Sloan and Thamb pipes)	Early Proterozoic Yavapi belt, 1.8–1.7 Ga (Hoffman, 1989)	14	7.9 ± 0.4	195

Table 2 (*continued*)

Region	Type and age structure	*n*	TG (°C/km)	Depth (km)
Late Precambrian and Phanerozoic structures				
Collisional belts				
South Mongolia, Dariganga Plateau, alkali-basalt volcanoes	Central Asian foldbelt, hercynides (Kovalenko et al., 1999)	4	9.4 ± 0.2	160
Accretionary belts				
Southeastern Siberia, Vitim Plateau alkali-basalt volcanoes	Central Asian foldbelt, ripheides (Kovalenko et al., 1999)	16	9.4 ± 0.3	175
Central Mongolia, Tariat Plateau alkali-basalt volcanoes	Central Asian foldbelt, Early Palaeozoic, caledonides (Kovalenko et al., 1999)	15	10.0 ± 0.4	160
Southeastern China, Quilin alkali-basalt volcanoes	Late Yangchuan Genozoic foldbelts (Fan and Hooper, 1989; Qi et al., 1995)	13	12.0 ± 0.5	110
Southeastern Australia, Bullenmerri, Bow Hill, New Wales, Leura, Delegate, and New Basalts alkali-basalt volcanoes	Palaeozoic Tasman belt (Simons et al., 1999)	23	10.8 ± 0.6	150
South America, Patagonia Plateau volcanoes, Pali-Aike alkali-basalt volcanoes	Phanerozoic foldbelt, sub-Andian lithosphere (Kempton et al., 1999)	17	9.0 ± 0.2	185
Phanerozoic oceanic structures				
Solomon Islands, alnoites of the Malaita island	Island arc (Coleman, 1966)	3	8.7 ± 0.2	170
Pacific Ocean, Hawaii, alkali basalts	Oceanic Plate hotspot (Sobolev and Nikogosyan, 1994)	5	11.7 ± 0.2	120

lith entrainment depths and the TG values in the mantle. This correlation does not practically express in Precambrian structures.

The maximum depths at which xenoliths were entrapped by alkali-basalt magma emplaced to Phanerozoic belts in Mongolia, southeastern China, southeastern Australia, and Hawaii are smaller than the depths of xenolith incorporation into kimberlites and alkali basalts in Precambrian structures and particularly in Archaean cratons. Here these depths reach 250 km. The minimum depths (110–120 km) were fixed in southeastern China and Hawaii. These data are in a good agreement with independent estimates of the melting depths of basaltic magmas and the thickness of the oceanic lithosphere in this region, which were obtained by Sobolev and Nikogosyan (1994). Their estimates of pressure and temperature for the primary melts of Hawaiian basalts obtained from melt inclusions in minerals and from the composition of basalt glasses, are 30–40 kbar and 1600–1470 °C, that corresponds the depth of 100–130 km.

For xenoliths from basalts in the southeastern part of South America, we obtained maximum depths comparable to those for xenoliths from kimberlites in Precambrian structures (about 180 km).

5. Discussion

The geotherms derived from xenoliths for Upper mantle under Archaean cratons differ from those in Archaean, Proterozoic collisional and accretionary belts, forming the following sequence from lower to higher temperatures: Archaean cratons → Archaean and Proterozoic collisional belts → Proterozoic accretionary belts. The geotherms from the first two types of structures on various continents are virtually identical (see Fig. 5). This may imply the absence of any spatial differentiation of thermal regimes in the Precambrian mantle during each of the (Archaean and Proterozoic) lithosphere evolution stages. In the Proterozoic, the hotter mantle may have influenced margin zones of Archaean cratons, as indicated, e.g., by higher TG values in the mantle beneath the southern Wyoming craton (Montana) near its boundary with the Yavapi accretionary belt (7.9 ± 0.3 °C/km) and beneath the westernmost part of the Kaapvaal craton (Zero; 7.5 ± 0.1 °C/km) near its boundary with the Early Proterozoic Case accretionary belt. In the mantle underlying the Arctic part of the North American platform, Canada (beneath the Archaean craton, which was reworked in the Early Proterozoic), the

Table 3
Equilibrium pressures and temperatures for garnet-bearing peridotite and pyroxenite xenoliths from various region and thermal gradient values in the Upper mantle

Sample	*P* (kbar)	*T* (°C)	TG (°C/km)	Reference	Sample	*P* (kbar)	*T* (°C)	TG (°C/km)	Reference
East Siberia									
Mir and Udachnaya pipes									
Uv71/75	36.8	900	7.2	1	Uv98/75	35.7	920	7.6	1
Uv1111	49.0	1185	7.1	1	Ud-1	53.7	1305	7.2	1
93/85	38.1	915	7.1	2	207/87	42.2	1025	7.2	2
556/80	37.8	910	7.1	2	557/80	46.0	1120	7.2	2
3-95	38.1	915	7.1	2	554/87	36.0	855	7.0	2
518/80	38.3	910	7.0	2	216/87	39.6	945	7.0	2
557/80	46.0	1120	7.2	2	4/83	38.9	970	7.3	2
199/82	43.7	1120	7.5	3	109/83	38.9	960	7.3	3
90/85	39.2	970	7.3	3	235/82b	38.3	955	7.3	3
79/749a	38.9	930	7.1	3	558/80	39.7	980	7.3	3
540/80′	39.7	960	7.1	3	94/85	36.0	900	7.4	3
61/83	40.5	980	7.1	3	10/83	38.8	925	7.0	3
92/85	38.4	940	7.2	3	235/82M	37.1	930	7.3	3
79/79M	38.9	940	7.1	3	555/80M	38.9	960	7.3	3
TUV-48	49,2	1180	7.1	4	TUV-7	36,1	865	7.1	4
TUV-65	36,0	885	7.2	4	TUV-150	39,1	895	6.7	4
U-756	53,4	1270	7.0	4	9292	55,3	1350	7.2	5
203/973	57.0	1380	7.1	5	225/576	68.2	1690	7.3	5
9208	53.9	1310	7.2	5	9222	53.0	1260	7.0	5
A-47	38.0	915	7.1	5	A-379	37.2	870	6.9	5
A-2	38.0	875	6.7	5	A-137	36.0	810	6.6	5
A-378	38.9	950	7.2	5	Uv624/86	38.2	950	7.3	6
Uv216/86	39.6	945	7.0	6	Uv255/75	59.6	1470	7.3	7
Uv53/91	45.2	1060	6.9	6	YB-198/76	46.6	1160	7.3	7
Ab-34	58.0	1445	7.3	8	AB-69	52.3	1340	7.0	8
AC-108	55.2	1350	7.2	8	AB-75	38.9	885	6.7	8
AB-93	45.0	1070	7.0	8	715	43.0	965	6.6	9
728/1	47.7	1110	6.8	9	728/2	42.3	975	6.8	9
Obnazhennaya pipe									
Ob-177	44.5	1160	7.6	5	Ob-152	49.3	1265	7.5	5
Ob-62	38.8	980	7.4	5	Ob-312	35.2	900	7.5	5
Ob-174	34.3	900	7.7	5	Ob-121	38.5	955	7.3	5
Ob-303	36.7	837	6.7	5	Ob-149	39.1	1015	7.6	5
Ob-100	46.5	1295	8.2	5	Ob-4	36.7	865	7.0	5
Obj-1	35.1	875	7.3	10	Obj′	38.6	955	7.7	10
47639	35.7	940	7.7	11	Yak1	41.0	1050	7.5	11
Northeastern Europe. Archangelsk region. Simnii bereg pipes									
Ar4-20	35.2	910	7.6	12	Ar4-22	37.8	965	7.5	12
K25-4	44.3	1065	7.1	12					
Finland. Kuopio and Kaavi pipes									
L1-A	46.0	1125	7.2	13	L29	43.6	1085	7.3	13
92/2	34.4	840	7.2	13	92/1	36.0	895	7.3	14
14.07/1	36.5	885	7.3	14	5.8/2	50.4	1260	7.4	14
14.01/1	45.8	1110	7.1	14	L44	42.5	1040	7.2	14
L51	43.5	1060	7.2	14	L60	48.7	1200	7.3	14
L66	40.7	1035	7.5	14	L57	41.1	1055	7.5	14
20HH	42.5	1030	7.1	14					

Table 3 (*continued*)

Sample	*P* (kbar)	*T* (°C)	TG (°C/km)	Reference	Sample	*P* (kbar)	*T* (°C)	TG (°C/km)	Reference
South Africa									
Premier, Kimberley, and Finsh kimberlite pipes									
FS-1	43.6	1075	7.3	10	FRB27	35.3	870	7.3	10
PHN2364a	42.4	1030	7.2	10	FRB28	42.3	1040	7.3	10
FRB81	50.9	1315	7.6	10	FRB85	52.7	1300	7.3	10
FRB1	53.1	1280	7.1	10	RVD181	47.3	1200	7.5	15
RVD155	43.4	1090	7.4	13	RVD183	50.3	1220	7.2	15
RVD101	56.8	1390	7.2	15	RVD146	48.4	1235	7.5	15
RVD101′	51.7	1275	7.3	15	8015	40.6	1030	7.5	16
73-180	43.3	1090	7.4	16	1755	39.5	980	7.3	16
1143	42.6	1050	7.2	16	1149	44.8	1120	7.4	16
1156	52.5	1240	7.0	16	1140	41.4	1040	7.4	16
BT-7	44.7	1080	7.1	16	JJG-147	46.9	1130	7.1	17
JJG-479	47.2	1115	7.0	17	JJG-545	57.3	1390	7.2	17
F-41	53.4	1280	7.1	17	F-45	48.3	1115	6.8	17
5	49.0	1155	7.0	18	7	56.7	1350	7.0	18
CK-1	40.6	975	7.1	19	CK-2	40.6	1020	7.4	19
CK-3	42.4	1080	7.5	19	CK-4	39.0	965	7.3	19
CB-4	47.6	1115	6.9	19	CB-6	46.1	1145	7.3	19
8015	40.6	1030	7.5	19	73-180	43.3	1090	7.4	19
JVS-73-63	54.0	1340	7.2	19	JVS-73-64	43.5	1080	7.3	19
JVS-73-76	42.7	1050	7.2	19	46	68.4	1660	7.2	20
48	45.5	1090	7.1	20	K2a	55.0	1335	7.2	21
K8a	41.4	990	7.1	21	K46	50.8	1240	7.2	21
K47	52.0	1235	7.0	21	K56	47.6	1160	7.2	21
XM-46	47.0	1135	7.1	7	XM-48	44.8	1090	7.2	7
Zero pipes									
K5/223	53.6	1362	7.5	22	K5/229	50.1	1283	7.5	22
K5/275	40.9	1048	7.5	22					
Botswana. Letlhakane pipes									
IST113	52.2	1270	7.2	23	ISL151	47.4	1150	7.2	23
ISL278	42.7	1070	7.4	23	ISL504	41.0	1015	7.3	23
ISL280	50.9	1305	7.5	23					
Limpopo. Venetia pipes									
32	51.7	1295	7.4	24	41	51.9	1305	7.4	24
49	52.9	1325	7.4	24	75	40.7	1060	7.6	24
3	37.9	1045	8.1	24					
Lesotho pipes									
PTH-102	43.7	1105	7.4	25	PTH-210	37.2	960	7.6	25
PTH-400	55.4	1395	7.4	25	PTH-404	47.6	1135	7.0	25
PTH-404	45.6	1170	7.5	25	PTH-407	46.8	1185	7.4	25
PTH-409	46.0	1195	7.6	25	PTH-204	44.1	1130	7.5	25
PTH-207	45.5	1170	7.5	25	PTH-410	51.3	1355	7.7	25
1359	46.6	1130	7.2	16	1363	45.2	1150	7.5	16
1031	47.2	1165	7.3	16	1361	44.2	1100	7.3	16
1362	45.2	1150	7.5	16	1032	41.8	1070	7.5	16
LBM38a	47.1	1180	7.4	17	LBM22b	45.3	1140	7.4	17
LBM22a	44.8	1130	7.4	17	BD2125	47.7	1175	7.2	7
Namibia									
Louwrensia pipes									
43	44.9	1120	7.4	26	42	45.9	1160	7.4	26
41	44.1	1105	7.4	26	37a	57.7	1485	7.5	26
35	44.2	1105	7.4	26	34	45.4	1140	7.4	26

(continued on next page)

Table 3 (*continued*)

Sample	*P* (kbar)	*T* (°C)	TG (°C/km)	Reference	Sample	*P* (kbar)	*T* (°C)	TG (°C/km)	Reference
Namibia									
Louwrensia pipes									
33a	48.8	1240	7.5	26	32	43.9	1100	7.4	26
25a	52.2	1325	7.5	26	24	48.6	1245	7.5	26
23	44.0	1100	7.4	26	22	48.9	1245	7.5	26
21	43.1	1095	7.5	26					
Hanaus pipes									
27	49.4	1070	7.3	26	26a	45.0	1130	7.4	26
22a	52.1	1455	8.2	26	20a	51.2	1435	8.2	26
19	45,4	1145	7,6	26	18	43,9	1120	7.5	26
17	42,5	1065	7.4	26	16	62,5	1580	7.4	26
12	55,5	1405	7.4	26	11	54.9	1392	7.5	26
9	54,3	1370	7.4	26	8a	49.7	1320	7.8	26
7	43.3	1090	7.4	26	6	48.5	1215	7.4	26
4	45,9	1160	7.4	26	3	50.7	1300	7.5	26
1	43,5	1095	7.4	26	KHA-46	49.1	1355	8.2	27
KHAL1	39.3	1020	7.6	27	KHA3	45.1	1240	8.1	27
KHA6	40.4	1035	7.5	27	KHA10	40.1	1035	7.6	27
KHA50	51.7	1390	7.9	27	KHA54	50.5	1355	7.8	27
KHA56	48.3	1325	8.1	27	KHA58	51.2	1320	7.6	27
KHA61	49.2	1325	7.9	27	KHA63	56.3	1440	7.5	27
KHA90	35.9	965	7.9	27	KHA91	49.3	1380	8.2	27
KHA92	50.6	1430	8.3	27	KHA93	48.8	1385	8.4	27
KHA103	38.0	990	7.6	27					
Anis-Kubub pipes									
KAK1	48.6	1245	7.5	27	KAK2	41.2	1070	7.6	27
KAK6	45.7	1195	7.7	27	KAK8	47.8	1240	7.6	27
KAK9a	44.7	1170	7.7	27	KAK9b	44.2	1130	7.5	27
KAK10	48.0	1255	7.7	27	KAK19a	49.7	1315	7.7	27
KAK19b	51.2	1340	7.7	27	KAK24a	48.3	1270	7.7	27
KAK24b	50.3	1335	7.8	27	KAK26	48.2	1230	7.5	27
KAK31	45.4	1155	7.5	27					
India. Vajrakurer pipes									
P3E	25.2	925	7.4	28	P3F2	43.6	1115	7.5	28
P3L2	39.9	995	7.3	28	P3-11	42.8	1080	6.8	28
P3-10	51.0	1270	7.3	28	P3-40	51.8	1290	6.7	28
P3L1	41.5	1040	7.4	28	P3-7	45.7	1100	6.5	28
P3BH1	53.5	1140	6.3	28	P3-39	52.4	1300	6.7	28
LA-L3	51.0	1270	7.3	28					
North America									
Montana pipes									
H67-28K3	46.3	1270	8.1	29	H67-28K2	49.5	1295	7.1	29
H67-28K4	35.2	990	8.3	29	H67-28K1	47.9	1250	7.0	29
Sloan pipes									
H69-15F	49.8	1300	7.6	29	H68-16B	37.7	915	7.2	29
CDZ-189	36.7	930	7.5	30	CDZ-112	28.3	865	9.0	30
Thamb pipes									
1078THM	48.0	1315	8.1	31	175THM	56.7	1400	7.3	31
8082THM	46.3	1340	8.5	31	CO73THM	47.6	1375	8.5	31
140THM	40.9	1160	8.4	31	DO76THM	45.4	1220	7.9	31
AO82THM	47.7	1285	7.9	31	RO77THM	49.5	1345	7.9	31
1078THM	48.5	1280	7.7	31	NO77THM	45.8	1205	7.7	31

Table 3 (*continued*)

Sample	*P* (kbar)	*T* (°C)	TG (°C/km)	Reference	Sample	*P* (kbar)	*T* (°C)	TG (°C/km)	Reference
Canada. Jericho pipe									
14-105	42.8	1080	7.4	32	26-12	43.8	1120	7.5	32
Id16Mx6	38.2	980	7.5	32	Id16Mx7a	38.5	990	7.5	32
Id16Mx7b	41.0	1050	7.5	32					
Canada. Somerset Island. Elwin Bay and Nikos pipes									
EGL5	53.6	1355	7.5	33	EGL8	48.8	1250	7.5	33
NK1-5	45.6	1170	7.5	34	NK2-3	37.0	940	7.5	34
NK2-10	43.4	1110	7.5	34	NK3-20	31.4	815	7.6	34
NK3-25	48.1	1250	7.6	34	NK1-2	43.8	1105	7.4	34
NK1-3	41.6	1050	7.4	34	NK1-6	44.5	1140	7.5	34
NK1-7	48.4	1255	7.6	34	NK1-17	42.1	1055	7.4	34
NK1-18	45.5	1170	7.5	34	NK2-7	40.5	1030	7.5	34

(1) Boyd, 1976; (2) Solov'eva and Zav'yalova, 1992; (3) Solov'eva et al., 1989; (4) Laz'ko and Sharkov, 1988; (5) Ukhanov et al., 1988; (6) Pokhilenko et al., 1976; (7) Sobolev et al., 1984; (8) Sobolev et al., 1976; (9) Sobolev et al., 1997; (10) Boyd, 1974; (11) McCulloch, 1989; (12) Sablukov et al., 2000; (13) Peltonen et al., 1999; (14) Kukkonen and Peltonen, 1999; (15) Danchin and Boyd, 1976; (16) Bishop et al., 1978; (17) Gurney et al., 1979; (18) Tsai et al., 1979; (19) Delaney et al., 1980; (20) Shee et al., 1982; (21) Rickard et al., 1989; (22) Shee et al., 1989; (23) Stiefenhofer et al., 1997; (24) Stiefenhofer et al., 1999; (25) Carswell et al., 1979; (26) Mitchell, 1984; (27) Franz et al., 1997; (28) Nehru and Reddy, 1989; (29) Hearn and Boyd, 1975; (30) Otter and Gurney, 1989; (31) Ehrenberg, 1979; (32) Kopylova et al., 1999; (33) Mitchell, 1979; (34) Schmidberger and Francis, 1999.

thermal regime appears to have been disturbed to an extent. Thus, the thermal parameters are close to the values in the mantle beneath Early Proterozoic collisional structures.

The inferred relationship between the thermal regimes in the mantle and types of Precambrian tectonic structures suggest that the TG values and geotherms derived from xenoliths characterize the thermal regimes that existed in the lithospheric mantle during the formation of tectonic structures of Precambrian crust, rather than the thermal regimes of kimberlite magmatism (Khiltova et al., 1995; Khiltova and Nikitina, 1997). In other words, these geotherms and TG values characterize the thermal state of the paleomantle. The established heterogeneities in the lithospheric mantle are relics largely preserved from ancient times. This is supported by age of mantle xenoliths (Richardson, 1989; Kinny et al., 1989; McCulloch, 1989) and by the fact that the TG values obtained for the mantle beneath the Kaapvaal craton from xenoliths of the 1180-Ma Premier kimberlite pipe (7.3 ± 0.2 °C/km; $n = 6$) are indistinguishable from the TG values (7.2 ± 0.2 °C/km; $n = 38$) derived from xenoliths in kimberlites of Mesozoic age (Kimberley and Finsh kimberlites). Xenoliths from the Early Proterozoic (1650 Ma) Zero pipe in the westernmost part of the same craton also yield low TG values typical of the mantle beneath Early Precambrian tectonic structures.

During incipient rifting stages, intraplate basaltic magmatism within cratons and Proterozoic mobile belts is unlikely to disturb the preexisting thermal structure of the mantle. This follows from data on the thermal regimes in the mantle beneath the Labait and Lashaine volcanoes, which are associated with the formation of the East African Rift but are located within the Archaean Tanzanian craton and the Proterozoic Mozambique belt of the collisional type, respectively.

Probably, stable regions of continental mantle appeared as early as the Archaean. The scales of these stable lithospheric blocks are difficult to surmise, but the fact that identical thermal regimes existed in the Archaean within the East Siberian platform, the Dharvar craton in India, and the Kaapvaal and Zimbabwe cratons in South Africa should be taken into account when dealing with this issue. The results of Sm–Nd and Re–Os isotopic studies (Pearson, 1999) indicate that mantle blocks beneath most cratons have been isolated from the convecting mantle since at least the Late or Middle Archaean and, for some cratons, since the Early Archaean. According to geochronological evidence, the lithospheric mantle underlying the Siberian, Kaapvaal, and Wyoming cratons has

Table 4
Equilibrium pressures and temperatures for garnet peridotite xenoliths in alkali basalts of various regions and thermal gradients in the mantle

Sample	*P* (kbar)	*T* (°C)	TG (°C/km)	Reference	Sample	*P* (kbar)	*T* (°C)	TG (°C/km)	Reference
Tanzania									
Labait Volcano									
GL4201	53.9	1450	7.9	1	GL4202	50.5	1325	7.7	1
G14203	51.1	1340	7.7	1	FH4203	51.1	1345	7.7	1
GL-XI	50.2	1315	7.7	1	GL-X9	53.1	1380	7.6	1
G14201	53.9	1450	7.9	1	G14202	50.5	1325	7.7	1
LB-24	52.9	1370	7.6	2	LB-53	50.4	1330	7.7	2
LB-24a	47.7	1240	7.6	2	KAT-17	52.2	1375	7.7	2
Lashaine Volcano									
775	50.3	1265	7.4	3	797	47.6	1215	7.5	3
797′	47.1	1220	7.6	3	796	48.5	1220	7.6	3
796′	48.1	1210	7.4	3	740	49.4	1230	7.3	3
794	49.2	1245	7.4	3	776	46.2	1205	7.7	3
782	56.0	1420	7.5	3	730	49.1	1275	7.6	3
Southern extremity of South America: Pali-Aike volcanoes									
TM2	49.9	1515	8.9	4	TM1	48.8	1480	8.9	4
BN4	51.1	1550	8.9	4	BN35	52.1	1575	8.9	4
L34	54.0	1645	8.9	4	LS101	53.0	1615	9.0	4
LC8	44.8	1405	9.2	5	LC11	50.8	1425	8.3	5
CP3	44.5	1350	8.9	5	CP8	44.3	1360	9.0	5
CP9	44.3	1385	9.1	5	CP11	45.0	1370	8.9	5
CP32	40.5	1300	9.5	5	CP34	42.8	1350	9.2	5
CP31	46.4	1410	8.9	5	CP84	42.5	1345	9.2	5
CP85	49.4	1505	8.9	5					
Southeastern Siberia: Vitim Plateau volcanoes									
313-1	45.5	1410	9.1	6	313-3	44.4	1380	9.1	6
313-4	42.8	1370	9.1	6	313-5	43.2	1410	9.6	6
313-8	50.0	1540	9.0	6	313-37	46.5	1445	9.1	6
313-54	51.9	1585	9.0	6	313-113	46.3	1500	9.6	6
313-103	45.5	1475	9.6	6	313-114	43.9	1490	9.2	6
313-74	48.7	1525	9.2	6	314-580	48.8	1545	9.4	6
SF93163	45.8	1465	9.4	6	SF93205	45.8	1440	9.2	7
SG96B13	45.0	1420	9.2	7	SF93174	44.1	1495	10.0	7
Mongolia									
Tariat Depression volcanoes									
130©	42.6	1420	9.8		MK-5	42.3	1480	10.2	8
A-18©	41.4	1385	9.8	8	A-18(r)	40.6	1395	10.1	8
198©	43.9	1500	10.1	8	197	35.6	1350	11.1	8
195	39.9	1295	9.6	8	MK17	43.4	1410	9.6	8
196	35.5	1235	10.2	9	69	42.3	1430	9.9	8
198(2)	43.3	1490	10.1	9	198(1)	46.7	1540	9.7	9
127	35.2	1295	10.8	9	224	40.5	1425	10.3	9
4334/11	45.5	1505	9.7	10	4334/14	41.8	1395	9.8	10
Dariganga Plateau volcanoes									
221	43.8	1400	9.4	8	204	47.5	1505	9.4	11
DB1	45.1	1475	9.6	12	DB3	46.7	1475	9.2	12

Table 4 (*continued*)

Sample	*P* (kbar)	*T* (°C)	TG (°C/km)	Reference	Sample	*P* (kbar)	*T* (°C)	TG (°C/km)	Reference
Southeastern Australia									
Delegate, Tumut-Ekumbene, Anakies, Leura, New Basalts, Bullenmari, Gnotuk, and New Wales volcanoes									
69-27	44.0	1460	9.8	13	R394h	39.3	1330	10.0	13
R394j	40.3	1355	9.9	13	2582c	35.8	1290	10.6	13
69-34	32.1	1350	12.4	13	324/38	31.9	1190	11.0	13
2688	34.9	1250	10.6	13	1	42.1	1450	10.1	14
1′	41.8	1545	10.9	14	2	31.3	1180	11.1	14
Gn35	35.4	1295	10.8	15	Gn35′	36.8	1330	10.7	15
Bm6	36.5	1325	10.7	15	Bm166′	40.2	1470	10.8	15
Bm166	32.5	1295	11.8	15	Bm167	35.5	1300	10.8	15
Gn639	29.9	1150	11.3	15	Gn649	30.0	1160	11.3	15
Dr10165	32.5	1230	11.1	15	Dr1065	32.5	1245	11.0	15
R49177	39.4	1440	10.8	16	R49178	39.9	1455	10.8	16
R49168	39.5	1450	10.8	16					
Southeastern China: Quilin Volcanoes									
Q9307	29.8	1220	12.1	17	Q9323	32.6	1285	11.6	17
Q9324	32.6	1295	11.6	17	Q8907	30.5	1255	11.2	17
Q9352	32.9	1260	11.2	17	Q9353	30.8	1310	12.5	17
Q9355	30.5	1240	12.2	17	Q9327	32.5	1296	11.8	17
Q935	29.8	1215	12.0	17	QL1	29.6	1242	12.3	17
QL8	25.5	1145	13.2	17	QL13	32.9	1368	12.2	17
QL21	29.1	1230	12.4	17					
Solomon Islands: Malaita Island									
3	42.4	1265	8.8	18	2	50.1	1438	8.4	18
1	39.6	1183	8.8	18					
Hawaiian Islands									
S-24	34.6	1366	11.6	19	S-6	32.6	1320	12.0	19
24	34.6	1364	11.6	19	31	29.7	1190	11.8	19
42	33.3	1277	11.3	19					

(1) Dawson et al., 1997; (2) Lee and Rudnick, 1999; (3) Reid et al., 1975; (4) Stern et al., 1989; (5) Kempton et al., 1999; (6) Ionov et al., 1993; (7) Glaser et al., 1999; (8) Kopylova et al., 1995; (9) Kopylova and Genshaft, 1991; (10) Laz'ko and Sharkov, 1988; (11) Nikiforova, 1998; (12) Ionov et al., 1999; (13) Irving, 1974; (14) Sutherland and Hollis, 1982; (15) Griffin et al., 1984; (16) Stolz, 1974; (17) Xu et al., 1996; (18) Beeson and Jackson, 1970; (19) Sobolev and Nikogosyan, 1994.

nearly the same age as the onset of the main crust-forming events. This fact, in the opinion of Pearson (1999), suggests either that the processes of mantle stabilization and crust formation are genetically connected or that, in order to be preserved, large fragments of continental crust require the stability of deep lithospheric roots, which have recently been often identified by seismic tomography. The problem of these roots beneath continents becomes particularly significant in light of the data presented here. Note the following two implications. First, the roots are ancient and are largely composed of relics of the Precambrian continental lithosphere. Second, the processes of thermal convection, which, undoubtedly, were repeatedly manifested, did not result in global mixing of the mantle material. It should be acknowledged, however, that these conclusions are only preliminary, because the data presented here on Archaean structures do not cover all ancient cratons.

The continental mantle underlying Phanerozoic accretionary belts is characterized by higher TG values. Among them, the coldest geotherms were established for the mantle beneath the accretionary belt along the Atlantic coast (southeastern South America) and Ripheides of the Central Asian fold-belt (the Vitim Plateau). The hottest ones are beneath the accretionary belt along the Pacific coast (the Tasmanian belt in southeastern Australia and

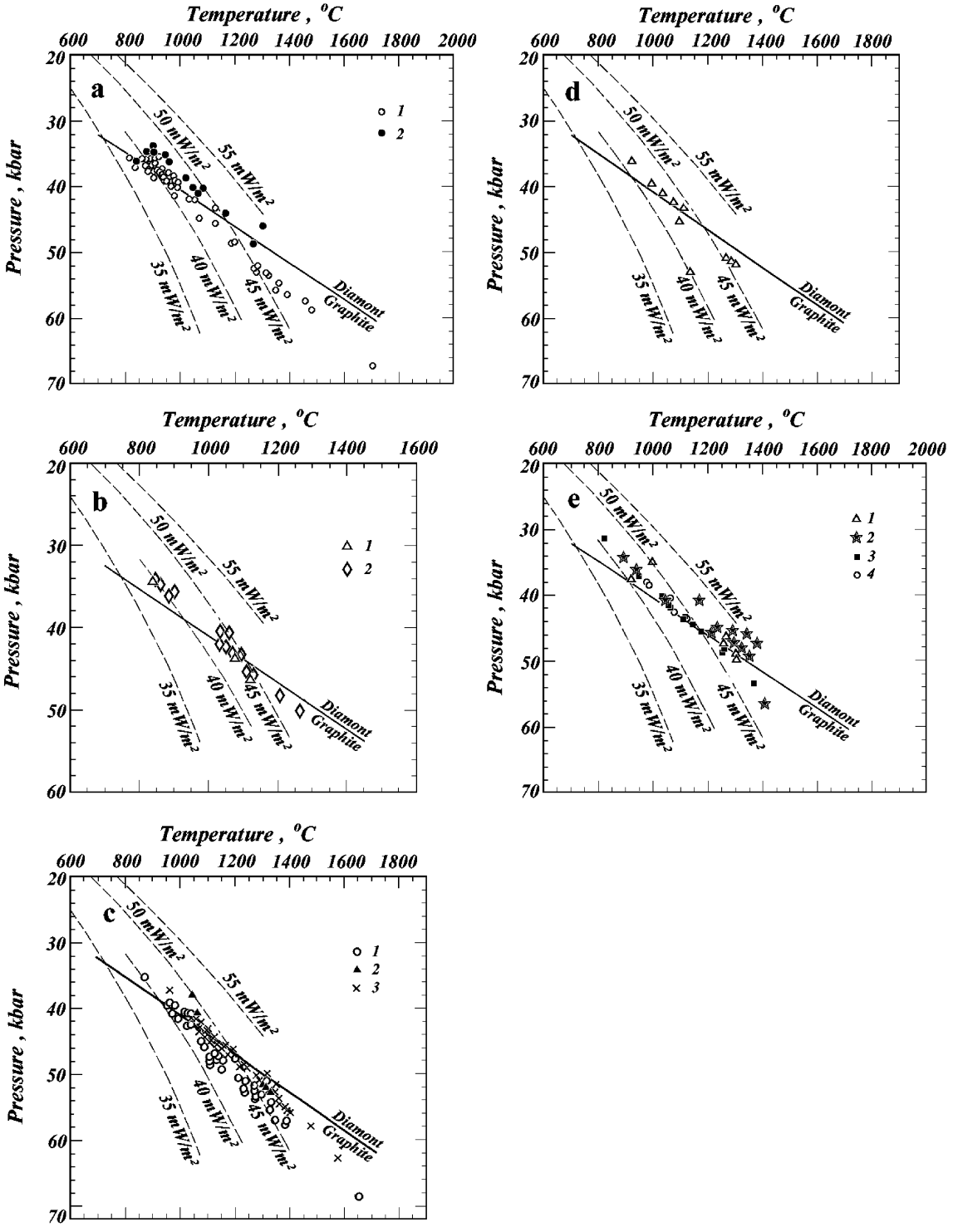
a
b
c
d
e
Temperature , °C
Pressure , kbar
50 mW/m²
55 mW/m²
40 mW/m²
45 mW/m²
35 mW/m²
Diamont
Graphite
1
2
3
4

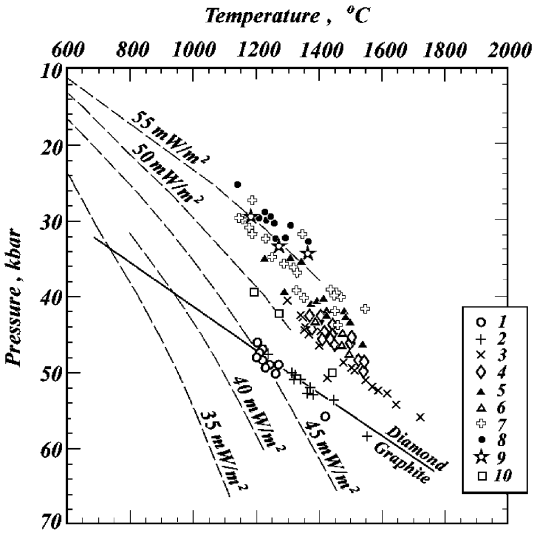

Fig. 4. The $P-T$ diagram from garnet peridotite xenoliths of alkali-basalt volcanoes: (1) Labait; (2) Lashaine, Tanzania; (3) Pali-Aike (southern extremity of South America); (4) Vitim Plateau (southeastern Siberia); (5) the Tariat depression, Mongolia; (6) the Dariganga plateau, Mongolia; (7) New Basalts, Bullenmerri, Gnotuk, and New Wales, southeastern Australia; (8) Quilin, Southeastern China; (9) Hawaiian Islands; (10) the Malaita island.

the Late Yangchuan foldbelt in China). The thermal regimes of the continental lithosphere at the Pacific margins of the Australian and Asian continents are similar to that of the oceanic lithosphere of the Hawaiian hotspot. Given that the ages of the alkali basalts containing the xenoliths are similar in all regions under discussion (Cenozoic), one can argue that the thermal heterogeneity of the mantle persisted until the Cenozoic and that the geodynamic settings of the accretionary belt development were more diverse in the Late Proterozoic and Phanerozoic than in the Early Precambrian.

Different trends in the relationship between the maximum depths at which xenoliths were entrapped by kimberlite and alkali-basalt magmas (or the minimum melting depths of these magmas) and the values in the mantle underlying Early Precambrian and Late Proterozoic–Phanerozoic structures, the relatively weak TG increase from the Archaean to the Early Proterozoic (see Fig. 6), the TG uniformity during each stage in the evolution of the Early Proterozoic mantle, and the significant increase and spatial differentiation in values of the Late Proterozoic and particularly Phanerozoic mantle are likely to indicate that the lithosphere dynamics changed at the boundary between the Early and Late Proterozoic or between the Precambrian and the Phanerozoic. It is interesting to note that changes in the thermal regime of the lithospheric mantle occurred at the Archaean/Early Proterozoic boundary. The data presented here are insufficient to reliably constrain the age of this boundary. In this context, it should be mentioned that the oldest supercontinent formed in the latest Archaean (about 2.6 Ga), and its breakup onset is dated at 2.45 Ga (Glebovitsky, 1996). There are reasons to assume that this was a time of dramatic change in global geodynamics, when the mechanism of plate tectonics started operating in full measure. An equally dramatic change took place in the Late Riphean, at the boundary with the Phanerozoic. A noteworthy distinct negative correlation between the minimums melting depths and mantle TG values is observed beneath Phanerozoic structures; this may be due to ascending convective flows of different temperatures, which were responsible for alkali-basalt magmatism in Phanerozoic structures. Possibly, similar convective phenomena took place in the Early Precambrian mantle; however, the differences between temperatures of convective flows were much smaller.

6. Conclusions

Using of the same garnet–orthopyroxene thermobarometer allows to carry out correctly comparison

Fig. 3. The $P-T$ diagram for garnet-bearing peridotite and pyroxenite xenoliths from kimberlite pipes in (a) the East Siberian platform [(1) pipes Mir and Udachnaya, (2) Obnazhennaya]; (b) Kuloisky [(1) Simnii bereg pipes] and Karelian [(2) Kaavi and Kuopio pipes] cratons; (c) South Africa [(1) pipes of the Premier, Kimberley, Finsch, Zero, Letlhakane kimberlite fields; (2) Limpopo, Central zone, Venetia pipes, (3) Lesotho (Lesotho-200, Kao, Thaba Putsoa, Letseng-la-Terae) and Namibian pipes (Louwrensia, Anis-Kubub, and Hanaus); (d) India (the Vajrakurer pipes); (e) North America [(1) Montana pipes, (2) Sloan and Thamb, (3) Elwin Bay and Nikos, (4) Jericho pipe]. Dash lines show the model continental geotherms corresponding to 35, 40, 45, 50, 55 mW/m^2 heat flows (Pollack and Chapman, 1977) and the solid curve—the polymorphic graphite–diamond transition (Bundy et al., 1961).

the thermal regimes in the mantle of different continents. Thus, it was established that:

1. Mantle geotherms and geothermal gradients, obtained on the base of data on P–T equilibrium conditions of deep xenoliths, correspond to the age of crust tectonic structures and respectively to the time of lithosphere stabilization. It can be suggested that the ancient structures of the upper mantle were preserved within continental roots;
2. The continental mantle under Neoproterozoic and Phanerozoic belts are characterized by significantly higher values of geothermal gradient compared to the mantle under Early Precambrian structures;
3. Lithosphere dynamics seems to change at the boundary between Early and Mezo-Neoproterozoic and Precambrian and Phanerozoic.

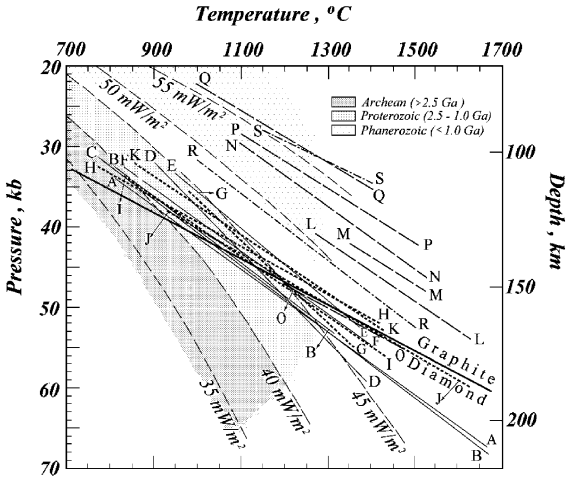

Fig. 5. Geotherms of the continental mantle underlying the following structures: (1) Archaean cratons (A–A, cratons in the basement of the East Siberian platform; B–B, Kuloisky and Karelian; C–C, Kaapvaal and Zimbabwe; D–D, West Dharvar; E–E, Wyoming; F–F, craton in the basement of the Arctic platform); (2) Precambrian collisional (G–G, Limpopo; H–H, West Olenek; I–I, Natal; J–J, Namaqualand; O–O, Mozambique) and accretionary (K–K, Yavapi) belts; (3) Late Proterozoic and Phanerozoic collisional and accretion belts (L–L, Palaeozoic belt of southern extremity of South America; M–M, ripheides and N–N, caledonides of Central Asian foldbelt; P–P, Tasmanian Palaeozoic; Q–Q, Late Yangchuan Cenozoic); (4) Phanerozoic oceanic structures: R–R, island arc (Solomon Islands); S–S, Hawaiian hotspot in the oceanic plate. The range of $P–T$ conditions derived from xenolith and xenocrysts suits in volcanic rocks that penetrate crust of Archaean, Proterozoic, Phanerozoic age (Poudjom Djomani et al., 2001) are shown by dotted fields.

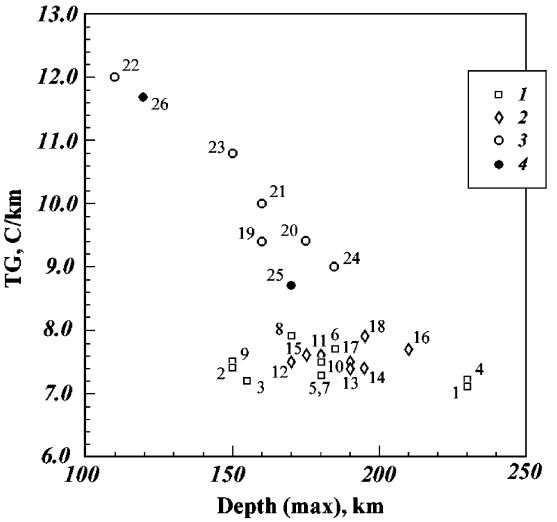

Fig. 6. TG averages in the mantle versus maximum depths at which mantle xenoliths were emplaced into kimberlites and alkali basalts in various Precambrian and Phanerozoic structures. (1) Archaean cratons [(1) in the basement of the East Siberian platform, (2) Kuloisky, (3) Karelian, (4) Kaapvaal, (5) Zimbabwe, (6) Tanzanian, (7) West Dharvar, (8) Wyoming, (9) Central Slave, (10) in the basement of the Arctic platform]; (2) Precambrian belts [collisional: (11) Limpopo; (12) West Olenek; (13) Natal; (14–16) Namaqualand: Louwrensia, Anis-Kubub, and Hanaus, respectively; (17) Mozambique; accretionary: (18) Early ProterozoicYavapi]; (3) Late Proterozoic and Phanerozoic belts [collisional: (19) hercynides of Central Asian belt; accretionary: (20–21) ripheides and caledonides of Central Asian belt, respectively; (22) Late Yangchuan Cenozoic; (23) Palaeozoic Tasmanian; (24) Palaeozoic belt at the southeastern extremity of South America]; (4) Phanerozoic oceanic structures [(25) the island arc, Solomon islands; (26) Hawaiian hotspot in the oceanic plate].

Acknowledgements

We thank A.O. Gliko for useful discussions. The manuscript was improved by constructive reviews by N.V. Sobolev. The research was supported by RFFI grant N 02-05-64822.

References

Akaogi, M., Akimoto, S., 1979. High pressure phase equilibria in a garnet lherzolite with special reference to Mg–Fe partitioning among constituent minerals. Phys. Earth Planet. Inter. 19, 31–51.

Akella, J., 1976. Garnet–clinopyroxene equilibria in the system $CaSiO_3$–$MgSiO_3$–Al_2O_3 and in natural mineral mixtures. Am. Mineral. 61, 589–598.

Anhaeusser, C.R., 1971. Cyclic volcanicity and sedimentation in the evolutionary development of Archean greenstone belts of shield areas. Spec. Publ. - Geol. Soc. Aust. 3, 57–70.

Beeson, M.H., Jackson, E.D., 1970. Origin of the garnet pyroxenite xenoliths at Salt Lake Crater Oahu. Spec. Pap. - Miner. Soc. Am. 3, 95–112.

Bishop, F.C., Smith, J.V., Dawson, J.B., 1978. Na, K, P and Ti in garnet, pyroxene and olivine from peridotite and eclogite xenoliths from African kimberlites. Lithos 11, 155–173.

Boyd, F.R., 1974. Ultramafic nodules from Frank Smith kimberlite pipe, South Africa. Year B. - Carnegie Inst. Wash. 73, 285–294.

Boyd, F.R., 1976. Inflected and noninflected geotherm. Year B. - Carnegie Inst. Wash. 75, 521–523.

Brey, G.P., Kohler, T., 1990. Geothermometry in four-phase lherzolites: II. New thermobarometers and practical assessment of existing thermobarometers. J. Petrol. 31, 1353–1378.

Bundy, F.R., Bovenkerk, H.P., Strong, H.M., Wentorf Jr., R.H., 1961. Diamond–graphite equilibrium line from growth and graphitization of diamond. J. Chem. Phys. 35, 383–391.

Carswell, D.A., Gibb, F.G.F., 1998. Evaluation on mineral thermometers and barometers applicable to garnet lherzolite assemblages. Contrib. Mineral. Petrol. 95, 499–511.

Carswell, D.A., Clarke, D.B., Mitchell, R.H., 1979. The petrology and geochemistry of ultramafic nodules from pipe 200, Northern Lesotho. In: Boyd, R.G., Meyer, H.O.A. (Eds.), The Mantle Sample: Inclusions in Kimberlites and Other Volcanics. Proc. Second Int. Kimberlite Conf., vol. 2, pp. 127–144.

Clark, S.P., Ringwood, A.E., 1964. Density distribution and constitution of the mantle. Rev. Geophys. 2, 35–88.

Cohen, L., Snelling, N.L., Vail, I.R., 1974. The Geochronology and Evolution of Africa. Clarendon Press, Oxford.

Coleman, P.S., 1966. The Solomon Islands as island arc. Nature 211, 1249–1251.

Cox, K.G., Smith, H.R., Beswetherick, S., 1989. Textural studies of garnet lherzolities: evidence of evolution origin from high-temperature harzburgites. In: Nixon, P.H. (Ed.), Mantle Xenolith, Geol. Soc. Australia Spec. Pub., vol. 14, Blackwell, Oxford, pp. 537–550.

Danchin, R.F., Boyd, F.R., 1976. Ultramafic nodules from premier kimberlite pipe, South Africa. Year B. - Carnegie Inst. Wash. 75, 531–538.

Dawson, J.B., James, D., Poslick, C., Holliday, A.M., 1997. Ultrabasic potassic low-volume magmatism and continental rifting in North–Central Tanzania: association with enhanced heat flow. Geol. Geofiz. 38 (1), 7–78 (in Russian English Translation: Russian Geol. Geophys, 38).

Delaney, J.S., Smith, I.V., Carswell, D.A., Dawson, I.B., 1980. Chemistry of micas from kimberlites and xenoliths: II. Primary and Secondary textured micas from peridotite xenoliths. Geochim. Cosmochim. Acta 44, 867–872.

Ehrenberg, S.N., 1979. Garnetiferrous ultramafic inclusions in minette from the Navajo volcanic field. In: Boyd, R.G., Meyer, H.O.A. (Eds.), The Mantle Sample: Inclusions in Kimberlites and Other Volcanics. Proc. Second Int. Kimberlite Conf., vol. 2, pp. 330–345.

Fan, Q., Hooper, P.R., 1989. The mineral chemistry of ultramafic xenoliths of Eastern China: implications for upper mantle composition and the paleogeotherms. J. Petrol. 30 (5), 111–1158.

Franz, L., Brey, G.P., Okrusch, M., 1997. Metasomatic reequilibration of mantle xenoliths from the Gibeon kimberlite province (Namibia). Geol. Geofiz. 38 (1), 245–260 (in Russian English Translation: Russian Geol. Geophys, 38).

Fyson, W.K., Helmstaedt, H., 1988. Structural patterns and tectonic evolution of supracrustal domains in Archean slave province, Canada. Can. J. Earth Sci. 25, 301–315.

Glaser, S.M., Foley, S.F., Gutner, D., 1999. Trace element compositions of minerals in garnet and spinel peridotite xenoliths from the Vitim volcanic field, Transbaikalia, Eastern Siberia. Lithos 48, 263–286.

Glebovitsky, V.A., 1996. Correlation and geodynamic interpretation of major events in Archean and Early Proterozoic structures of Laurasia. Geol. Geofiz. 3 (1), 42–53 (in Russian English Translation: Sov. Geol. Geophys, 3).

Glebovitsky, V.A., 1997. The Early Precambrian of Russia. Harwood Academic, Amsterdam.

Green, T.H., Adam, J., 1991. Assesment of the Garnet–clinopyroxene Fe–Mg exchange thermometer using new experimental data. J. Metam. Geol. 9, 341–348.

Griffin, W.L., Wass, S.I., Hollis, I.D., 1984. Ultramafic xenoliths from bullenmerri and Gnotuk Maars, Victoria, Australia: petrology of subcontinental crust–mantle transition. J. Petrol. 25 (1), 53–83.

Gurney, J.J., Harris, J.W., Rickard, R.S., 1979. Silicate and oxide inclusions in diamonds from the finsh kimberlite pipe. In: Boyd, F.R., Meyer, H.O.A. (Eds.), Kimberlites, Diatremes and Diamonds: Their Geology, Petrology and Geochemistry. Proc. Second Int. Kimberlite Conf., vol. 1. American Geophysical Union, Washington DC, pp. 1–15.

Harley, S.S., 1984a. The solubility of alumina in orthopyroxene coexisting with garnet in FeO–MgO–Al2O3–SiO2 and CaO–FeO–MgO–Al2O3–SiO2 systems. J. Petrol. 25, 665–696.

Harley, S.S., 1984b. Comparison of garnet–clinopyroxene geobarometer with experimental studies and applications to natural assemblages. J. Petrol. 25, 697–712.

Hearn Jr., B.C., Boyd, F.R., 1975. Garnet peridotite xenoliths in Montana, USA kimberlite. Phys. Chem. Earth 9, 247–255.

Hoffman, P.F., 1989. Precambrian geology and tectonic history of North America. The Geology of North America: A. An Overview of the Geol. Sci. America, Boulder, Colorado, 447–509.

Ionov, D.A., Ashchepkov, I.V., Shtosh, Kh.G., Zek, Kh.A., Vitt-Aikshen, G., 1993. Garnet peridotite xenoliths of the Vitim volcanic field, trans-Baikal region: petrology and geochemistry of garnet–spinel peridotites from the transition zone of the subcontinental mantle. In: Bogatikov, O.A., et al. (Eds.), Magma-

tizm Riftov I Skladchatykh Poyasov (Magmatism of Rifts and Foldbelts) Nauka, Moscow, pp. 169–211.

Ionov, D.A., Griffin, W.L., O'Reilly, S.Y., 1999. Off-cratonic garnet and spinel peridotite xenoliths from Dsun-Bussular, SE Mongolia. Proc. VII Int. Kimb. Conf., Red Roof Design, Cape Town, South Africa, pp. 383–390.

Irving, A.J., 1974. Geochemical and high pressure experimental studies of garnet pyroxenite and pyroxene granulite xenoliths from the delegate basaltic pipes, Australia. J. Petrol. 15, 1–40.

Kempton, P.D., Lopez-Escobar, L., Hawkesworth, C.J., Pearson, D.G., Wright, D.W., Ware, A.J., 1999. Spinel garnet lherzolite xenoliths from Pali-Aike: Part I. Petrography, mineral chemistry and geothermobarometry. Proc. VII Int. Kimb. Conf., Red Roof Design, Cape Town, South Africa, pp. 403–414.

Khiltova, V.Ya., Nikitina, L.P., 1997. Precambrian tectonic structures and thermal state of the underlying mantle. Dokl. Akad. Nauk 357 (3), 384–386.

Khiltova, V.Ja., Nikitina, L.P., Berkovsky, A.N., Khiltova, E.Yu., 1995. The Precambrian crust structures and the upper mantle thermal state of ancient platforms. Proc. IX General. Meet. MAEGS, St. Petersburg, Russia, pp. 51–52.

Kinny, P.D., Compston, W., Britow, J.W., Williams, I.S., 1989. Archean mantle xenolith in a Permian kimberlite: two generations of kimberlite zircon in Jwaneng DK2, Southern Botswana. In: Ross, J., et al. (Eds.), Kimberlite and Related Rocks. Proc. Fourth Int. Kimberlite Conf., GSA, Spec. Publ. 14, vol. 2. Blackwell, Oxford, pp. 833–834.

Kondie, K., 1981. Archean Greenstone Belts. Elsevier, Amsterdam.

Kopylova, M.G., Genshaft, Yu.S., 1991. Petrology of garnet–spinel xenoliths from Cenozoic basalts in Mongolia Akad. Izv. Akad. Nauk SSSR, Ser. Geofiz. 5, 36–59 (in Russian).

Kopylova, M.G., O'Reilly, S.Y., Genschaft, Yu.S., 1995. Thermal state of the lithosphere beneath central Mongolia: evidence from deep-seated xenoliths from the Shavaryn-Saram volcanic centre in the Tariat depression, Hangai, Mongolia. Lithos 36, 243–255.

Kopylova, M.G., Russell, J.K., Cookenboo, H., 1999. Mapping the lithoshere beneath the North Central slave craton. Proc. VII Int. Kimb. Conf., Red Roof Design, Cape Town, South Africa, pp. 468–479.

Kovach, V.P., Smelov, A.P., Kotov, A.B., Safronov, A.F., Pavlushin, A.D., 2000. Structure and crust-forming events in the buried basement of the East Siberian Platform: the first review of Nd isotopic studies. Petrologia 4, 442–457 (in Russian).

Kovalenko, V.I., Yarmolyuk, V.V., Kovach, V.P., Budnikov, S.V., Zhuravleva, D.Z., Kozakov, I.K., Kotov, A.B., Rytsk, E.Y., Sal'nikova, E.B., 1999. Implications of crust-forming magmatic processes for the development of the Central Asian foldbelt: Sm–Nd isotope data. Geotektonika 3, 21–42 (in Russian).

Kukkonen, I.T., Peltonen, P., 1999. Xenolith-controlled geotherm for the central Fennoscandian Shield: implications for the lithosphere–astenosphere relations. Tectonophysics 304, 301–315.

Laz'ko, E.E., Sharkov, E.V. (Eds.), 1988. Magmaticheskie gornye porody. Ul'traosnovnye porody (Igneous Rocks: Ultrabasic Rocks). Nauka, Moscow, pp. 326–328.

Lee, C.T., Rudnick, R.L., 1999. Compositionally stratified cratonic lithosphere: petrology and geochemistry of peridotite xenoliths from Labait volcano, Tanzania. Proc. VII Int. Kimb. Conf. Red Roof Design, Cape Town, South Africa, pp. 503–524.

MacGregor, J.D., 1974. The system $MgO–Al_2O_3–SiO_2$: solubility of Al2O3 in enstatite for spinel and garnet peridotite compositions. Am. Mineral. 59, 110–119.

McCulloch, M.T., 1989. Sm–Nd systematics in eclogite and garnet peridotite nodules from kimberlites: implications for the early differentiation of the earth. In: Ross, J., et al. (Eds.), Kimberlites and Related Rocks. Proc. Fourth Int. Kimberlite Conf., GSA, Spec. Publ. 14, vol. 2. Blackwell, Oxford, pp. 864–876.

Mitchell, R.H., 1979. Ultramafic xenoliths from Elwin Bay kimberlite: the first Canadian palaeogeotherm. Can. J. Earth Sci. 14, 1202–1210.

Mitchell, R.H., 1984. Garnet lherzolites from Hanaus-I and Louwrensia kimberlites of Namibia. Contrib. Mineral. Petrol. 86, 178–188.

Moller, A., Mezger, K., Schenk, V., 1998. Crustal age domains and the evaluation of the continental crust in the Mozambique belt of Tanzania: combined Sm–Nd, Rb–Sr and Pb–Pb isotopic evidence. J. Petrol. 39, 749–783.

Nehru, C.E., Reddy, A.K., 1989. Ultrabasic xenoliths from Vajrakurer kimberlites, India. In: Ross, J., et al. (Eds.), Kimberlites and Related Rocks. Proc. Fourth Int. Kimberlite Conf., GSA, Spec. Publ. 14, vol. 2. Blackwell, Oxford, pp. 745–759.

Neymark, L.A., Nemchin, A., Rozen, O.M., Serenko, V.P., Spetsius, Z.V., Shuleshko, I.K., 1992. The Sm–Nd systematics in the lower crust xenoliths from Yakutian kimberlites. Dokl. Akad. Nauk 327, 374–378 (in Russian).

Nikiforova, N.F., 1998. Geotherms in the upper mantle of the trans-Baikal region and Mongolia in the Late Cenozoic. Izv. Vyss. Ucebn. Zaved., Geol. Razved. 1, 18–25 (in Russian).

Nikitina, L.P., 1986. Termodinamika Tverdykh Rastvorov Silikatov (Thermodynamics of Silicate Solid Solutions). Nauka, Leningrad. In Russian.

Nikitina, L.P., 2000. Garnet–orthopyroxene and garnet–clinopyroxene thermobarometers for the mantle xenoliths. In: Glebovitsky, V.A., Dech, V.I. (Eds.), Theophrastus Contributions to Advanced Studies in Geology: 3. Capricious Earth: Models and Modelling of Geologic Processes and Objects. Theophrastus, St. Petersburg, Athens, pp. 44–53.

Nikitina, L.P., Ivanov, M.V., 1992. Geologicheskaya termobarometriya na osnove reaktsii mineraloobrazovaniya s uchastiem faz peremennogo sostava (Geological Thermobarometry Based on the Mineral-Forming Reaction with Participation of the Variable-Composition Phases). Nedra, St. Petersburg. In Russian.

Otter, M.L., Gurney, J.J., 1989. Mineral Inclusions from the Sloan diatremes, Colorado–Wyoming state line kimberlite district, North America. In: Ross, J., et al. (Eds.), Kimberlites and Related Rocks. Proc. Fourth Int. Kimberlite Conf., GSA, Spec. Publ. 14, vol. 2. Blackwell, Oxford, pp. 1042–1053.

Pearson, A.I., 1999. The age of continental roots. Lithos 48, 171–194.

Peltonen, P., Huhma, H., Tuni, M., Shimizu, N., 1999. Garnet peridotite xenoliths from kimberlites of Finland: nature of the

continental mantle at the Archean craton–Proterozoic mobile belt transition. Proc. VII Int. Kimb. Conf., Red Roof Design, Cape Town, South Africa, pp. 664–676.

Perkins, D., Holland, T.J.B., Newton, R.C., 1980. The Al_2O_3 contents of enstatite in equilibrium with garnet in the system MgO–Al_2O_3–SiO_2 at 15–40 kbar and 900–1600 °C. Contrib. Mineral. Petrol. 78, 99–109.

Peters, S.W., 1991. Regional Geology of Africa. Lecture Notes in Earth Sciences, vol. 40. Springer-Verlag, Berlin.

Pokhilenko, N.P., Sobolev, N.V., Sobolev, V.S., Lavrent'ev, Yu.G., 1976. Xenolith of diamond-bearing ilmenite–pyrope lherzolite from the Udachnaya kimberlite pipe, Yakutia. Dokl. Akad. Nauk SSSR 231 (2), 438–441 (in Russian).

Pollack, H.N., Chapman, D.S., 1977. On the regional variation of heat flow, geotherms and lithospheric thickness. Tectonophysics 38, 279–296.

Poudjom Djomani, Y.H., O'Reilly, S.Y., Griffin, W.L., Morgan, P., 2001. The density structure of subcontinental lithosphere through time. Earth Planet. Sci. Lett. 184, 605–621.

Qi, Q., Taylor, L.A., Zhou, X., 1995. Petrology and geochemistry of mantle peridotite xenoliths from SE China. J. Petrol. 36, 55–79.

Rai, S.S., Rajgopala Sarma, P.V.S.S., Prakasam, K.S., Rao, V.K., 1996. Seismic evidence for thick and underplated Late Archean crust of Eastern Dharvar craton. Proc. Indian Acad. Sci. (Earth Planet. Sci.) 105 (4), 431–439.

Reid, A.M., Donaldson, C.H., Brown, R.W., Ridley, W.J., Dawson, J.B., 1975. Mineral chemistry of peridotite xenoliths from the Lashaine volcano, Tanzania. Phys. Chem. Earth (9), 525–543.

Richardson, S.N., 1989. Definitive as ever a reply to "Archean diamond xenocrysts in kimberlites—how definitive is the evidence". In: Ross, J., et al. (Eds.), Kimberlites and Related Rocks. Proc. IV Int. Kimb. Conf., GSA, Spec. Publ. 14, vol. 2. Blackwell, Oxford, pp. 1070–1075.

Rickard, R.S., Harris, J.W., Gurney, J.J., Cardoso, P., 1989. Mineral inclusions in diamonds from Koffiefontein Mine. In: Ross, J., et al. (Eds.), Kimberlites and Related Rocks. Proc. Fourth Int. Kimberlite Conf., GSA, Spec. Publ. 14, vol. 2. Blackwell, Oxford, pp. 1054–1062.

Ryabchikov, I.D., Brey, G.P., Bulatov, V.K., 1993. Near solidus melts in carbonated peridotites at 50 kbar. In: Bogatikov, O.A., et al. (Eds.), Rift and Fold Belt Magmatism. Nauka, Moscow, pp. 265–274. In Russian.

Sablukov, S.M., Sablukova, L.I., Shavirina, M.V., 2000. Mantle xenoliths from the kimberlite deposits of round diamonds of Zimnii bereg districts, Arkhangelsk province. Petrologia 8 (5), 518–548 (in Russian).

Schmidberger, S.S., Francis, D., 1999. Nature of the mantle root beneath the North American craton: mantle xenolith evidence from Somerset Island kimberlites. Lithos 48, 195–217.

Shee, S.R., Gurney, J.J., Robinson, D.N., 1982. Two diamond-bearing peridotite xenoliths from finsh kimberlite, South Africa. Contrib. Mineral. Petrol. 81, 148–156.

Shee, S.R., Bristow, J.W., Bell, D.R., Smith, C.B., Allsopp, H.L., Shee, P.B., 1989. The petrology of kimberlites, related rocks and associated xenoliths from Kuruman province, South Africa. In: Ross, J., et al. (Eds.), Kimberlites and Related Rocks. Proc. Fourth Int. Kimberlite Conf. GSA, Spec. Publ. 14, vol. 1, pp. 60–83.

Simons, F.J., Zielhuis, A., van der Hilst, R.D., 1999. The deep structure of the Australian continent from surface wave tomography. Lithos 48, 17–45.

Sobolev, A.V., Nikogosyan, I.K., 1994. Magmatism petrology of long-lived mantle jets: Hawaii, Pacific, and Reunion Island, Indian Ocean. Petrologia 2 (2), 131–168.

Sobolev, N.V., Botkunov, A.I., Lavrentyev, Yu.G., Usova, L.V., 1976. New data on the composition of minerals, associated with diamonds. Geol. Geofiz. 12, 3–14 (in Russian).

Sobolev, N.V., Pokhilenko, N.P., Yefimova, E.S., 1984. Diamond-bearing xenoliths in kimberlites and the problem of diamond origin. Geol. Geofiz. 12, 63–80 (in Russian).

Sobolev, N.V., Kaminsky, F.V., Griffin, W.L., Yefimova, E.S., Win, T.T., Ryan, C.G., Botkunov, A.I., 1997. Mineral inclusions in diamonds from the Sputnik kimberlite pipe. Lithos 39, 135–157.

Solov'eva, L.V., Zav'yalova, L.L., 1992. Stratification of the mantle lithosphere under the Siberian platform from petrological and geophysical data. Geodin. Issled. 14, 21–34 (in Russian).

Solov'eva, L.V., Lipskaya, V.I., Barankevich, V.G., 1989. The comagmatic series of garnet clinopyroxenites, olivine Websterites, and lherzolites from the Udachnaya Pipe. In: Vladimirov, B.M. (Ed.), Problemy kimberlitovogo magmatizma (Problems of the Kimberlite Magmatism). Nauka, Novosibirsk, pp. 212–239.

Stern, C.R., Saul, S., Skewes, M.A., Futa, K., 1989. Garnet peridotite xenoliths from the Pali-Aike alkali basalts of Southernmost South America. In: Ross, J., et al. (Eds.), Kimberlites and Related Rocks. Proc. Fourth Int. Kimberlite Conf., GSA, Spec. Publ. 14, vol. 2. Blackwell, Oxford, pp. 735–744.

Stiefenhofer, I., Viljoen, K.S., March, J.S., 1997. Petrology and geochemistry of peridotite xenoliths from the Letlhaekane kimberlites, Botswana. Contrib. Mineral. Petrol. 127 (1/2), 147–159.

Stiefenhofer, J., Viljoen, K.S., Tainton, K.M., Hannweg, G.W., 1999. The petrology of a mantle xenolith suite from Venetia, South Africa. Proc. VII Int. Kimb. Conf., Red Roof Design, Cape Town, South Africa, pp. 836–845.

Stolz, A.S., 1974. Garnet websterites and associated ultramafic inclusions from a nepheline mugearite in Walcha area, New South Wales, Australia. Mineral. Mag. 48, 167–179.

Sutherland, F.L., Hollis, J.D., 1982. Mantle–lower crust petrology from inclusions in basaltic rocks in Eastern Australia—an outline. J. Volcanol. Geotherm. Res. 14 (1), 1–20.

Tsai, H., Meyer, H.O.A., Moreau, J., Milledge, H.J., 1979. Mineral inclusions in diamond: premier, jagersfontein and finsh kimberlites, South Africa, and Williamson Mine, Tanzania. In: Boyd, F.R., Meyer, O.A. (Eds.), Kimberlites, Diatremes and Diamonds: Their Geology, Petrology and Geochemistry. Proc. Second Int. Kimberlite Conf., vol. 1, pp. 16–27.

Ukhanov, A.V., Ryabchikov, I.D., Khar'kiv, A.D., 1988. Litosfernaya mantiya Yakutskoi kimberlitovoi provintsii (Lithospheric

mantle of the Yakutian kimberlite province). Nauka, Moscow. In Russian.

Xu, X., O'Reilly, S.Y., Zhou, X., Griffin, W.L., 1996. A xenolith-derived geotherm and the crust–mantle boundary at Qilin, Southeastern China. Lithos 38, 41–62.

Yamashita, K., Creaser, R.A., Jensen, J.E, Heamen, L.M., 2000. Origin and evolution of mid-to late Archean crust in the Hanikahimajuk lake area, Slave province, Canada; evidence from U–Pb geochronological, geochemical and Nb–Pb isotopic data. Precambrian Res. 99, 197–224.